Statistical-based model development with surrogate rainfall fields and its use to assess typhoon rain hazard for coastal region of mainland China

X.Z. Cui
Assistant Professor, School of Civil and Environmental Engineering, Harbin Institute of Technology, Shenzhen, China. Email: cuixizhong@hit.edu.cn

J.Y. Gu
Assistant Professor, College of Civil Engineering and Architecture, Dalian University, Dalian, China. Email: jiyang_gu@163.com

H.P. Hong
Professor, Department of Civil and Environmental Engineering, University of Western Ontario, London, Canada. Email: hhong@uwo.ca

ABSTRACT: Tropical cyclones (TCs) could cause intense rainfall along the coastal region of mainland China. The modeling of rainfall intensity could be carried out using snapshots of the rainfall intensity field obtained from satellite data such as those from the Tropical Rainfall Measuring Mission (TRMM) satellite data. In the present study, both the precipitation radar TRMM (PR-TRMM) data and the Microwave Imager (TMI) TRMM (TMI-TRMM) data that affect onshore sites in mainland China are considered to develop rainfall intensity models. To augment the database for the model development, surrogates of the snapshots are generated using an efficient iterative simulation algorithm and applying the discrete orthogonal S-transform. The simulated surrogates for the seed snapshots follow the same marginal distribution and power spectral density distribution. Empirical models of the rainfall intensity are developed using the surrogates so to increase the sample size. For the development, the TC rainfall intensity field is represented as a superposition of the axisymmetric, asymmetric, and topographic components. This consideration is guided by the parametric hurricane rain model (PHRaM) available in the literature. It is shown that the rainfall intensity inferred from the snapshots from PR-TRMM is greater than that from the snapshots from TMI-TRMM. The developed models are used in a simulation framework to map TC rain hazard (in terms of the return period value of the annual maximum accumulated rain per day).

1. INTRODUCTION

China experiences significant rainfall-induced damage. The heavy rainfall could be caused by the occurrence and passing of tropical cyclones (TCs) (i.e., typhoons) (Chen et al. 2010). The rain hazard assessment and mapping for mainland China are extensively discussed and presented in the literature by considering all mechanisms or types of heavy rainfall (Luo et al. 2020). However, it appears that the TC rain hazard mapping for the coastal region of mainland China is not available in the literature. This is in contrast with typhoon wind hazard mapping for the same region, which was presented in several studies using different wind field models (e.g., Xiao et al. 2011; Hong et al. 2016; Sheng and Hong 2020).

The modeling and prediction of the TC rainfall intensity is a necessary step to assess accumulated TC rain hazard. The TC rainfall intensity is influenced by the storm size, intensity, sea-surface temperatures, vertical wind shear, and topographic effect (Lonfat et al. 2004, 2007; Tuleya et al. 2007; Chen et al. 2010). Two popular statistical-based models were proposed to model the rainfall intensity: the rainfall climatology and persistence model (R-CLIPER) (Tuleya et al. 2007) and the parametric hurricane rain model (PHRaM) (Lonfat et al. 2007). An assessment of the performance of R-CLIPER and PHRaM for landfalling TCs affecting the U.S., as well as other rainfall intensity models, was presented in Brackins and Kalyanapu (2020). The assessment of the rainfall asymmetries and the relationship between the TC intensity and rainfall distribution for landfalling TCs affecting mainland China was investigated by Yu et al. (2017) using the Fourier series. Gu et al. (2022) calibrate the model parameters by adopting PHRaM and using PR-TRMM and TMI-TRMM data. They also combine the developed rainfall intensity model with historical and synthetic TC tracks to estimate the return period value of the accumulated rainfall in 24 hours for a few locations in the coastal region of mainland China. The estimated values are compared to the gauge data.

One of the critical aspects of developing a statistical-based rainfall intensity model is the availability of a sufficient number of sampled rainfall fields that represent the realization of the random rainfall intensity fields for different combinations of the TC parameters. Unfortunately, the data collection is a resource-intensive task, and the available samples of the rainfall intensity field are limited, considering the possible combinations of the TC parameters. An alternative is to generate surrogates based on observed rainfall intensity fields that are viewed as samples of stochastic fields to augment the data. The generation and application of surrogates were extensively elaborated in Schreiber and Schmitz (1996). They proposed an iterative amplitude adjusted Fourier transform (IAAFT) algorithm to generate surrogates. The generation of multi-dimensional nonstationary surrogates was also presented in Hong et al. (2021) and Zhou et al. (2021). The one considered in Zhou et al. (2021) is based on the efficient and non-redundant discrete orthonormal wavelet transform (DOST) (Stockwell 2007). However, it seems that the generation and use of surrogates of the TC rainfall intensity fields have not been explored in the literature.

In the present study, we propose to generate surrogates of the rainfall field by using the rainfall intensity fields from PR-TRMM and TMI-TRMM as the target or seed rainfall fields. The two-dimensional DOST is employed to decompose the seed rainfall field and to generate the surrogate. The generation of surrogates is focused on the rainfall intensity fields of the landfalling TC events affecting mainland China. The generated surrogates have the same marginal cumulative distribution as that of the seed rainfall field and retain the spectral characteristics of the seed field in the DOST domain. We then calibrate the model parameters by adopting PHRaM and using PR-TRMM/ TMI-TRMM with surrogates. The calibration follows the same procedure that is used by Gu et al (2022) for developing the model based only on the actual data.

A preliminary map for the accumulated annual maximum rainfall hazard in the coastal region of mainland China considering different return periods is given to show the applicability of the developed model based on both seed and surrogates.

2. RAINFALL INTENSITY SNAPSHOTS AND GENERATION OF SURROGATES

2.1. TC Rainfall intensity snapshots considered

The instantaneous rainfall intensity field inferred from the PR data or TMI data obtained through the TRMM program (Simpson et al. 1988; Kummerow et al. 2000) could be used to overcome the shortage of rainfall intensity field data from surface stations. The considered snapshots from TRMM program in the present study and focused on mainland China are the same as those described in Gu et al. (2022). The details and criteria used in selecting and processing the considered snapshots are given in the same reference as well. The snapshots consist of 614 snapshots of rainfall fields from 148 TCs that are found in the PR-TRMM dataset, and 933 snapshots from 151 TCs that are extracted from the TMI-TRMM dataset.

Two samples of snapshots of the rainfall fields, one from PR-TRMM and the other from TMI-TRMM, are shown in Figures 1a and 1b. The samples shown in Figure 1 are considered as samples from the stochastic fields.

Note that the snapshots of rainfall fields from TRMM have been used as the basis to develop R-CLIPER model (Marks et al. 2002; Tuleya et al. 2007) and PHRaM (Lonfat et al. 2007). However, the number of snapshots of the rainfall intensity fields for the combinations of TC parameters is relatively limited for the possible combinations of TC parameters. This is especially the case considering that each snapshot is a single realization of the stochastic rainfall field. To increase the number of snapshots to be used to calibrate an instantaneous rainfall intensity model, in the present study, the generation of the surrogate is carried out based on each observed snapshot of the rainfall fields. Both the original snapshots and their surrogates are used to calibrate the parameters for the PHRaM model focused on the landfalling TC affecting mainland China. The procedure to generate surrogate and model calibration is described in the following sections.

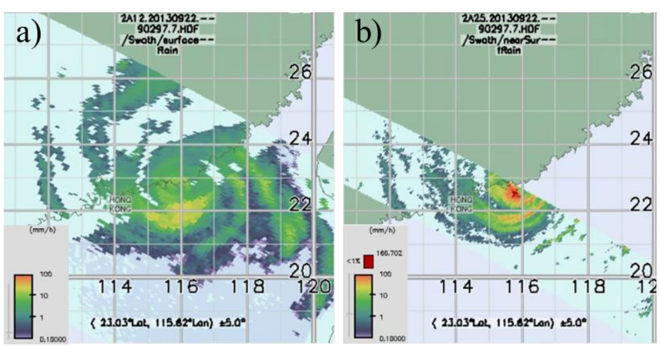

Figure 1: Two snapshots of instantaneous rainfall intensity fields for the same instance (extracted from TRMM)

2.2. Generation of surrogates based on discrete orthogonal S-transform

Schreiber and Schmitz (1996) proposed an iterative amplitude adjusted Fourier transform (IAAFT) algorithm to generate surrogates for hypothesis testing. The generated surrogate for a given time history (or signal) is to have the Fourier amplitude spectrum (or power spectral density) equal to that of the original signal. Also, the values of the surrogate are the same as those of the original signal but with their order shuffled. The algorithm is popular and has been extended by others (Venema et al. 2006, Hong et al. 2021, Zhou et al. 2021). In particular, Zhou et al. (2021) used the discrete orthonormal S-transform (DOST) (Stockwell 2007) to simulate the inhomogeneous random corrosion surface by applying the iterative power and amplitude correlation (IPAC) algorithm (Hong et al. 2021a,b). The use of DOST, which is efficient and easy to interpret, is adopted in the present study to generate surrogates of the inhomogeneous non-Gausian rainfall field. This increased the number of snapshots of the instantaneous TC rainfall fields that could be used to calibrate rainfall intensity model (i.e. PHRaM).

According to Stockwell (2007), for a one-dimensional field, DOST maps a discrete N-point space series to an N-point space-wavenumber representation by using N orthonormal basis functions, $D_{[\beta]}(x_k; p, q)$, where the basis function is given by,

$$D_{[\beta]}(x_k; p, q) = \frac{ie^{-i\pi q}}{\sqrt{\beta}} \times \frac{\{e^{-i2\pi(k/N-q/\beta)(p-\beta/2-1/2)} - e^{-i2\pi(k/N-q/\beta)(p+\beta/2-1/2)}\}}{2\sin[\pi(k/N-q/\beta)]} \quad (1)$$

in which $x_k = k\Delta_x$; the indices p and q are used to indicate the frequency band $f_p = p/(N\Delta_x)$ and space localization $x_q = q\Delta_x$, respectively; β indicates the width of the frequency band. Stockwell (2007) suggested that $q = 0, 1, \ldots, \beta - 1$, and p and β can be selected by using octave sampling. This leads to $(p; q; \beta)|_{m=0} = (0; 0; 1)$, $(p; q; \beta)|_{m=1} = (1; 0; 1)$, and $(p;q;\beta)\big|_{m=2,\ldots,\log_2(N)-1} = (2^{m-1}+2^{m-2}; 0, \ldots, 2^{m-1}-1; 2^{m-1})$, where m is the octave number.

In Eq. (1), N equals a power of 2. The total number of the complex basis functions based on the combinations of p and q is $N/2$. The use of the $N/2$ basis function is similar to the Fourier transform and is justified since the basis function is conjugate symmetric (i.e., $D^*_{[\beta]}(x_k; p, q) = D_{[\beta]}(x_k; -p, q)$), where the asterisk denotes the complex conjugate. An illustration of the partition used in DOST is presented in Figure 2.

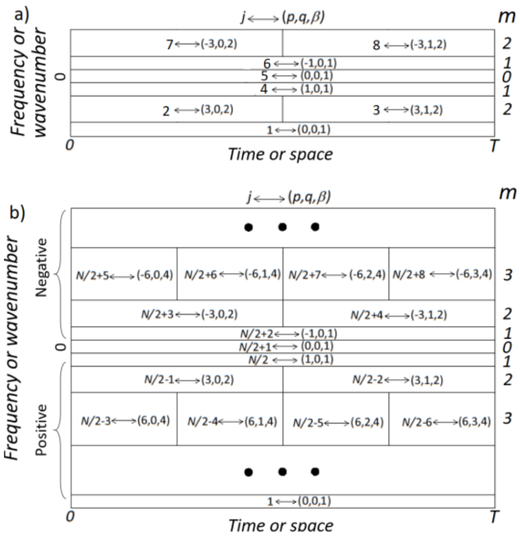

Figure 2: Relation between the double indices (p,q) to a system of single index j for DOST: a) Case for N = 8, and b) N equals a power of 2 (Modified after Zhou et al. 2021).

In anticipation of dealing with the multi-dimensional random field, it is convenient to simplify the double indices (p,q) (i.e., $(p;q;\beta)$) to a single index j, as shown in Figure 2a for the case when N = 8, and in Figure 2b in general when N equals an integer power of 2. The figure indicates that each partition depicted in Figure 2 that corresponds to a combination of the two indices (p,q) is represented by a number in a single index system. The octave number m = 0 to 3 is also shown in the plot. The correspondence between j and $(p;q;\beta)$ for the general case is illustrated in Figure 2b. Based on the adopted single index system, the notation for the basis function $D_{[\beta]}(x_k;p,q)$ is then represented by $D_{[\beta]}(x_k;j)$.

Based on the above, the DOST pair for a one-dimensional signal can be written as,

$$y_{\mathscr{DS}}(j) = \left(1/N\right)\sum_{k=0}^{N-1} y(x_k) D_{[\beta]}(x_k;j) \tag{2}$$

and,

$$y(x_j) = \sum_{j=0}^{N-1} \left|y_{\mathscr{DS}}(j)\right| D^*_{[\beta]}(x_k;j) e^{i\arg\left(y_{\mathscr{DS}}(j)\right)} \tag{3}$$

here $y_{\mathscr{DS}}(j)$ is the DOST coefficients of $y(x_k)$. Note that Eqs. (2) and (3) can be evaluated using the fast Fourier transform (FFT) for computational efficiency; the DOST coefficients for a one-dimensional real-valued signal are conjugate symmetric for positive and negative frequency (Wang and Orchard 2009).

Similar to the two-dimensional FT, the two-dimensional DOST (i.e., 2D-DOST) is also separable (Stockwell 2007). This facilitates its use in dealing with a field $y(x_1, x_2)$ in two-dimensional space. Let $\{y(x_{k_1}, x_{k_2})\}_N$, denote the sampled $y(x_1, x_2)$ at discrete points, where $x_{k_1} = k_1\Delta_{x1}$, $x_{k_2} = k_2\Delta_{x2}$, k_h = 0, 1, 2, …, N_h -1 (h = 1, 2), $N = N_1N_2$, Δ_{xh} is the sampling interval for x_h, and N_h is the total number of sampled points (considered to be the power of 2) along x_{k_h}. The 2D-DOST pair can be written as,

$$y_{\mathscr{DS}}\left(j_1, j_2\right) = \frac{1}{N_1}\frac{1}{N_2}\sum_{k_1=0}^{N_1-1}\sum_{k_2=0}^{N_2-1} y(x_{k_1}, x_{k_2}) D_{[\beta]}(x_{k_1};j_1) D_{[\beta]}(x_{j_2};j_2) \tag{4}$$

$$y_s(x_{k_1}, x_{k_2}) = \sum_{j_1=0}^{N_1-1}\sum_{j_2=0}^{N_2-1} \left|y_{\mathscr{DS}}\left(j_1, j_2\right)\right| D^*_{[\beta]}(x_{k_1};j_1) D^*_{[\beta]}(x_{k_2};j_2) e^{i\arg\left(y_{\mathscr{DS}}\left(j_1, j_2\right)\right)} \tag{5}$$

where j_1 = 0, …, N_1-1, and j_2 = 0, …, N_2-1; the orthogonal basis functions are defined above.

By using the IPAC algorithm with 2D-DOST, the generation of surrogates for a given sample of the rainfall field $\left\{y(j_1\Delta_{x1}, j_2\Delta_{xn})\right\}_N$ is as follows:

1) Calculate $y_{\mathscr{DS}}\left(j_1, j_2\right)$ using Eq. (4) for the given seed rainfall field $\left\{y(j_1\Delta_{x1}, j_2\Delta_{xn})\right\}_N$, sort $\left\{y(j_1\Delta_{x1}, j_2\Delta_{xn})\right\}_N$ in ascending order and store it in $\left\{\zeta(j)\right\}_N$. Sample $\theta\left(j_1, j_2\right)$ which is independent and uniformly distributed between 0 and 2π.
2) Calculate the power corrected field $y_{PC}(x_{k_1}, x_{k_2})$ by using the right-hand side of Eq. (5) but with $\arg\left(y_{\mathscr{DS}}\left(j_1, j_2\right)\right)$ replaced with

$\theta(j_1, j_2)$. Find the rank of $y_{PC}(x_{k_1}, x_{k_2})$ denoted as $r(x_{k_1}, x_{k_2})$, for all combinations of k_1 and k_2.

3) Assign the amplitude corrected field $y_{AC}(x_{k_1}, x_{k_2}) = \zeta(r(x_{k_1}, x_{k_2}))$, calculate its DOST coefficient $y_{\mathcal{DS}}(j_1, j_2)$, and let $\theta(j_1, j_2) = \arg\left(y_{\mathcal{DS}}(j_1, j_2)\right)$.

4) if $\sum_{k_1}\sum_{k_2}\left[y_{PC}(x_{k_1}, x_{k_2}) - y(x_{k_1}, x_{k_2})\right]^2 / \sum_{k_1}\sum_{k_2}\left[y(x_{k_1}, x_{k_2})\right]^2$ is greater than a specified tolerance value ε, Repeat Steps 2) to 3), otherwise, take $y_{AC}(x_{k_1}, x_{k_2})$ as the surrogate.

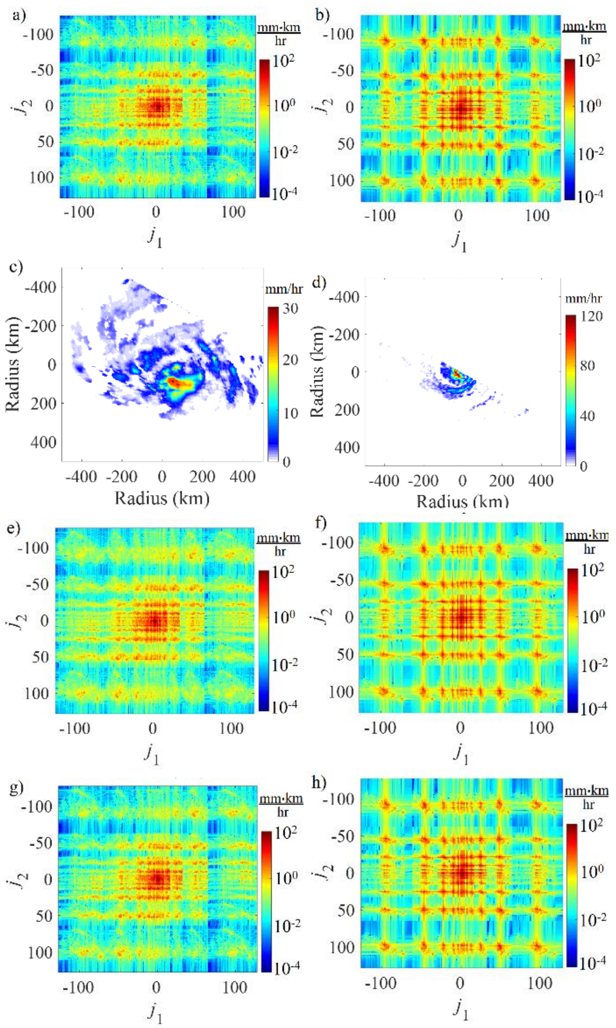

Figure 3: a) and b) Amplitude of the seed rainfall field; c) and d) typical simulated surrogates; e) and f) Amplitude of the DOST coefficient of the surrogates shown in c) and d); g) and h) the mean of the amplitude of DOST coefficient for 50 generated surrogates.

For the numerical analysis presented in the following, ε equal to 2×10^{-3} is employed. A preliminary analysis indicates that the use of the IPAC algorithm for a seed rainfall intensity field with a large area of almost zero rainfall intensity could generate surrogates that are significantly different from the seed rainfall intensity field (cannot reach the convergency). Consequently, it was decided that the generation of the rainfall field is to be carried out by only considering cells with at least 0.01 of the maximum rainfall intensity, I_{max}. For example, by considering each rainfall field presented in Figure 1 as the target (or seed) random fields and using the described algorithm with the mentioned criterion, the evaluated amplitude of the DOST coefficients by applying Eq. (4) are shown in Figures 3a and 3b, respectively. Using the obtained amplitude of the coefficient and the simulation steps, typical surrogates for the rainfall fields shown in Figure 1 are illustrated in Figures 3c and 3d. The amplitude of the DOST coefficients of the surrogates are shown in Figures 3e and 3f, indicating that they mimic well the DOST amplitude of seed field. The correlation coefficient between $\left|y_{\mathcal{DS}}(j_1, j_2)\right|$ for the seed rainfall field and the surrogate equals 0.992 and 0.993 if the rainfall intensity field shown in Figures 1a and 1b are considered, respectively.

Moreover, by generating 50 surrogates for each of the rainfall intensity fields shown in Figure 1, The average of the amplitude of the DOST coefficients of the surrogates is calculated. The obtained averages are shown in Figures 3g and 3h. The correlation coefficient between $\left|y_{\mathcal{DS}}(j_1, j_2)\right|$ for the seed rainfall intensity field and the mean of the amplitude of the DOST coefficients of the 50 surrogates equals 0.9981 if the rainfall intensity field shown in Figure 1a is considered. This value becomes 0.9988 if the rainfall field shown in Figure 1b is considered. This indicates that the surrogates are consistent with the seed rainfall intensity field in terms of the amplitude of DOST coefficients (i.e., power distribution in the time and frequency domain). Note that the marginal probability distribution function of the surrogates is the same as that of the seed field by design (see Step 3 of the algorithm).

3. CALIBRATING MODEL PARAMETERS

PHRaM (Lonfat et al. 2007) is a modified version of R-CLIPER model (Marks and DeMaria 2001; Tuleya et al. 2007) by including the effect of wind shear (Chen et al. 2006) and the orographic effect. For the model development focused on mainland China, the same procedures used by Gu et al. (2022) in obtaining the parameters for rainfall intensity $I(r,\alpha)$ that is expressed as,

$$I(r,\alpha)=\max\begin{pmatrix} 0,(1+\gamma_{Top}(r,\alpha))I_0(r) \\ +\sum_{k=1}^{2}a_k(r/r_m)\cos(k\alpha) \\ +\sum_{k=1}^{2}b_k(r/r_m)\sin(k\alpha)+\varepsilon(r/r_m) \end{pmatrix} \tag{6}$$

where $I_0(r)$ is the axisymmetric component; $a_k(r/r_m)$ and $b_k(r/r_m)$ are the coefficients to model the asymmetric component of the rainfall caused by wind shear; $\varepsilon(r/r_m)$ is the residual that is assumed to be normally distributed. $I_0(r)$ is modeled using,

$$I_0(r)=\begin{cases} I_0+(I_m-I_0)\dfrac{r}{r_m}, & r/r_m\le 1 \\ I_m\exp\left(-\left(\dfrac{r}{r_m}-1\right)^n/\rho_e\right), & r/r_m>1 \end{cases} \tag{7}$$

where n and ρ_e are model parameters, $I_m=a_{Im}+1.20b_{Im}V_m$, and $I_0=a_{I0}+1.25b_{I0}V_m$ and V_m is the surface wind speed (i.e., maximum wind speed at 10 m height above the ground surface). For simplicity, r_m is taken equal to the radius at which the maximum wind speed occurs, R_{max}.

It is considered that $\gamma_{Top}(r,\alpha)$ shown in Eq. (6) depends on the topography and the TC wind field,

$$\gamma_{Top}(r,\alpha)=\begin{cases} 1\times(|lift|/100), & lift>0 \\ -0.2\times(|lift|/100), & lift\le 0 \end{cases} \tag{8}$$

where the *lift* (m) is the difference in the elevation (see additional detailed discussions on the modeling of $I(r,\alpha)$ given in Gu (2021)).

According to CMA (GB/T19201 2006), TC can be grouped into one of the six Intensity Categories (IC) shown in Table 1. The calibration of the PHRaM for landfalling TCs affecting mainland China is carried out for three groups of intensity class: Group 1 contains IC 1, Group 2 contains IC 2 and 3, and Group 3 contains IC 4, 5, and 6. For easy reference, these three groups are referred to as GC1, GC2, and GC3, respectively.

Table 1: Intensity Category according to CMA (GB/T19201 2006).

Name, (IC)	*Wind speed (m/s)*
Tropical depression, 1	*10.8-17.1*
Tropical storm, 2	*17.2-24.4*
Severe tropical storm, 3	*24.5-32.6*
Typhoon, 4	*32.7-41.4*
Severe typhoon, 5	*41.5-50.9*
Super typhoon, 6	*≥51.0*

Note: The wind speed representing the near-surface maximum 2-minute mean wind speed near the TC center.

For the rainfall intensity model development, ten surrogates for each considered snapshot are generated. The surrogates and the seed snapshots are all used for developing the model. The model coefficients for $I_0(r)$ (referred to as Case PR) are estimated through regression analysis and using the snapshots from PR and their corresponding surrogates. Similarly, the model coefficients (i.e., referred to as Case TMI) are estimated based on snapshots from TMI and their corresponding surrogates. The obtained model coefficients for $I_0(r)$ for Case PR and Case TMI are shown in Table 2. Further details on the estimation as well as the parameters for $a_k(r/r_m)$ and $b_k(r/r_m)$ are given in Gu (2022), and the mean and standard deviation of the residuals $\varepsilon(r/r_m)$ are presented in Table 3. It is observed that the standard deviation decreases as r/r_m increases. The decrease in the standard deviation can be explained by noting that the rainfall intensity decreases as $\varepsilon(r/r_m)$ increases. The mean is very small as compared to the standard deviation and could be considered to be zero, indicating that the model is unbiased.

Table 2: Intensity Category according to CMA (GB/T19201 2006).

Group	Case	Parameters					
		a_{I0}	b_{I0}	a_{Im}	b_{Im}	n	ρ_e
GC1	PR	-2.28	0.22	0.18	0.06	0.29	1.62
	TMI	-3.25	0.25	0.31	0.04	0.41	2.10
GC2	PR	1.07	0.04	-2.37	0.22	0.58	1.91
	TMI	-1.94	0.11	-1.86	0.14	0.83	4.07
GC3	PR	-0.14	0.02	0.02	0.17	1.44	7.72
	TMI	-0.21	0.04	0.02	0.13	1.41	7.48

Table 3: Intensity Category according to CMA (GB/T19201 2006).

Case and grouped intensity categories		Mean $\mu_\varepsilon = a_{\mu\varepsilon} + b_{\mu\varepsilon} \times (r / r_m)$		Standard deviation $\sigma_\varepsilon = a_{\sigma\varepsilon} + b_{\sigma\varepsilon} \times (r / r_m)$	
		$a_{\mu\varepsilon}$	$b_{\mu\varepsilon}$	$a_{\mu\sigma}$	$b_{\mu\sigma}$
PR	GC1	-0.142	0.0148	3.355	-0.2183
	GC2	-0.063	0.0111	6.605	-0.4748
	GC3	-0.701	0.0889	11.707	-0.9073
TMI	GC1	-0.123	0.0145	2.047	-0.0823
	GC2	0.041	-0.0003	3.231	-0.1573
	GC3	-0.217	0.0356	6.019	-0.4021

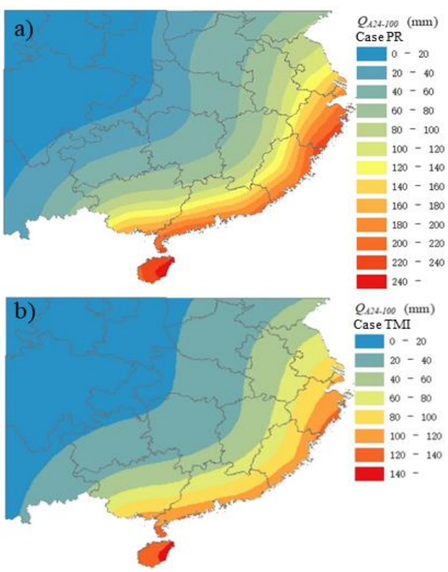

Figure 4: Mapped accumulated annual maximum rainfall hazard: 100-year return period value of Q_{A24} a) if rainfall intensity model for PR is used, b) if rainfall intensity model for TMI is used.

4. EVALUATION OF THE TC RAIN HAZARD

Using the rain hazard estimation procedure at a site (Gu et al. 2022) and considering the developed rainfall intensity models in the previous sections, the rainfall hazard, in terms of annual maximum rainfall amount within 24 hours, Q_{A24}, in the coastal region of mainland China is estimated and mapped. The procedure consists of the combined use of the rainfall intensity models, and synthetic TC tracks to estimate the T-year return period value of Q_{A24}, Q_{A24-T}, based on the simulation technique.

For the estimation and mapping, we consider the square grid system with a separation between the grid of 0.5° covering the coastal region. The mapped hazard is shown in Figure 4. The results shown in the figure indicate that the obtained values for Case PR are greater than those for Case TMI. The ratio of the former to the latter is about 1.6. This discrepancy could be explained by noting that the rainfall intensity for the snapshots from PR is consistently greater than that from TMI. Also, the standard deviation of the residual for Case PR is about twice that for Case TMI. The standard deviation also affects the estimated extreme value of the accumulated rain hazard.

5. CONCLUSIONS

An approach to generate surrogates for the rainfall intensity fields by using the snapshots from PR-TRMM and TMI-TRMM as the seed field is proposed. The generated surrogates could be used to augment available TC rainfall intensity fields so to increase the sample size. Both the original rainfall intensity fields as well as their surrogates for the TCs affecting onshore sites in the coastal region of mainland China are used as samples to evaluate the parameters for the TC rainfall intensity model (i.e., PHRaM).

To show the application of the models for the TC rain hazard assessment, we combine the developed rainfall intensity models, and synthetic TC tracks to estimate Q_{A24-T}. We mapped $Q_{A24-100}$ for part of the coastal region in mainland China. These maps show that the spatial variation of $Q_{A24-100}$ is relatively smooth.

It was observed that the estimated $Q_{A24-100}$ using the model developed based on the snapshots from TMI-TRMM is about 60% of that obtained using model developed based on the snapshots from PR-TRMM. This inconsistency reflects the differences in the rainfall intensity between TMI-TRMM and PR-TRMM.

6. ACKNOWLEDGMENT

We gratefully acknowledge the financial support received from the Harbin Institute of Technology, Western University, and the Natural Sciences and Engineering Research Council of Canada (RGPIN-2016-04814, for HPH).

7. REFERENCES

Brackins, J. T., & Kalyanapu, A. J. (2020). Evaluation of parametric precipitation models in reproducing tropical cyclone rainfall patterns. Journal of Hydrology, 580, 124255.

Chen, L., Li, Y., & Cheng, Z. (2010). An overview of research and forecasting on rainfall associated with landfalling tropical cyclones. Advances in Atmospheric Sciences, 27(5), 967-976.

GB/T19201 (2006) China meteorology administration, grade of tropical cyclones (GB/T19201-2006), Beijing: China Standards Press. (in Chinese)

Gu, J. (2021). Estimation of tropical cyclone rain hazard for sites in coastal region of mainland China (Doctoral dissertation, The University of Western Ontario (Canada)).

Gu, J., Cui, X., & Hong, H. (2022). A Statistical-Based Model for Typhoon Rain Hazard Assessment. Atmosphere, 13(8), 1172.

Hong, H. P., Cui, X. Z., & Qiao, D. (2021). An algorithm to simulate nonstationary and non-Gaussian stochastic processes. Journal of Infrastructure Preservation and Resilience, 2(1), 1-15.

Hong, H. P., Cui, X. Z., & Zhou, W. X. (2021). A model to simulate multidimensional nonstationary and non-Gaussian fields based on S-transform. Mechanical Systems and Signal Processing, 159, 107789.

Hong, H. P., Li, S. H. & Duan, Z. D. (2016). Typhoon wind hazard estimation and mapping for coastal region in mainland China. Natural Hazards Review, 17(2), 04016001.

Kummerow, C., Simpson, J., Thiele, O., Barnes, W., Chang, A. T. C., Stocker, E., ... & Nakamura, K. (2000). The status of the Tropical Rainfall Measuring Mission (TRMM) after two years in orbit. Journal of applied meteorology, 39(12), 1965-1982.

Lonfat, M., Marks Jr, F. D., & Chen, S. S. (2004). Precipitation distribution in tropical cyclones using the Tropical Rainfall Measuring Mission (TRMM) Microwave Imager: A global perspective. Monthly Weather Review, 132(7), 1645-1660.

Lonfat, M., Rogers, R., Marchok, T., & Marks Jr, F. D. (2007). A parametric model for predicting hurricane rainfall. Monthly Weather Review, 135(9), 3086-3097.

Luo, Y., Sun, J., Li, Y., Xia, R., Du, Y., Yang, S., ... & Li, M. (2020). Science and prediction of heavy rainfall over China: Research progress since the reform and opening-up of new China. Journal of Meteorological Research, 34(3), 427-459.

Marks, F. D., G. Kappler, and M. DeMaria, 2002: Development of a tropical cyclone rainfall climatology and persistence (RCLIPER) model. Preprints, 25th Conf. on Hurricanes and Tropical Meteorology, San Diego, CA, Amer. Meteor. Soc., 327–328.

Schreiber, T., & Schmitz, A. (1996). Improved surrogate data for nonlinearity tests. Physical review letters, 77(4), 635.

Sheng, C., & Hong, H. P. (2020). On the joint tropical cyclone wind and wave hazard. Structural Safety, 84, 101917.

Simpson, J., Adler, R. F., & North, G. R. (1988). A proposed tropical rainfall measuring mission (TRMM) satellite. Bulletin of the American meteorological Society, 69(3), 278-295.

Stockwell, R.G. (2007). A basis for efficient representation of the S-transform. Digit. Signal Process, 17(1), 371-393.

Tuleya, R. E., DeMaria, M., & Kuligowski, R. J. (2007). Evaluation of GFDL and simple statistical model rainfall forecasts for US landfalling tropical storms. Weather and forecasting, 22(1), 56-70.

Venema, V., Ament, F., & Simmer, C. (2006). A stochastic iterative amplitude adjusted Fourier transform algorithm with improved accuracy. Nonlinear Processes in Geophysics, 13(3), 321-328.

Wang, Y., & Orchard, J. (2009). Fast discrete orthonormal Stockwell transform. SIAM Journal on Scientific Computing, 31(5), 4000-4012.

Xiao, Y.F., Duan, Z.D., Xiao, Y.Q., Ou, J.P., Chang, L. and Li., Q.S. (2011). Typhoon wind hazard analysis for southeast China coastal regions. Structural Safety. 33:4-5, 286-295.

Yu, Z., Wang, Y., Xu, H., Davidson, N., Chen, Y., Chen, Y., & Yu, H. (2017). On the relationship between intensity and rainfall distribution in tropical cyclones making landfall over China. Journal of Applied Meteorology and Climatology, 56(10), 2883-2901.